Carbon nanotube gated lateral resonant tunneling field-effect transistors

D. P. Wang[a]
Department of Physics, Brown University, Providence, Rhode Island 02912

B. R. Perkins, A. J. Yin, A. Zaslavsky, J. M. Xu, and R. Beresford
Division of Engineering, Brown University, Providence, Rhode Island 02912

G. L. Snider
Department of Electrical Engineering, University of Notre Dame, Notre Dame, Indiana 46556

(Received 22 June 2005; accepted 16 August 2005; published online 4 October 2005)

We have produced a lateral resonant tunneling field-effect transistor using a Y-junction multiwalled carbon nanotube as the dual gate on a narrow channel etched from a modulation-doped GaAs/AlGaAs heterostructure. When the Y-junction nanotube is negatively biased, electrons traveling from source to drain along the channel face a voltage-tunable electrostatic double-barrier potential. We measured the three-terminal $I_{DS}(V_{DS}, V_{GS})$ characteristics of the device at 4.2 K and observed gate-induced structure in the transconductance and negative differential resistance in the drain current. We interpret the data in terms of resonant tunneling through one-dimensional subbands confined by a self-consistently calculated electrostatic potential. © *2005 American Institute of Physics*. [DOI: 10.1063/1.2089177]

Carbon nanotubes (CNTs) have generated a great deal of interest for use in novel devices due to their small size and high current-carrying capabilities. Using CNTs as the conducting channel material to build field effect transistor (FET) devices has been widely investigated.[1–3] In this letter, we use a Y-junction multiwalled CNT as the dual gate to create a lateral electrostatic double-barrier quantum well and control the conductance in a high mobility modulation-doped GaAs/AlGaAs channel. The principle of operation is analogous to lithographically defined metal-gated lateral resonant tunneling FET (LARTFET) reported previously.[4,5]

Our devices are built on top of a modulation-doped GaAs/AlGaAs heterostructure grown by molecular-beam epitaxy, consisting of a 1 μm GaAs buffer layer, a 15 nm undoped AlGaAs spacer layer, a 40 nm Si-doped AlGaAs layer, a 10 nm undoped AlGaAs layer, and a 20 nm undoped GaAs cap layer. The Al content is 28% in all AlGaAs layers. A two-dimensional electron gas (2DEG) is confined at the heterointerface with electron density $n_{2D}=3.85\times10^{11}$ cm^{-2} and cm^2/V s at 4.2 K, characterized by standard van der Pauw magnetoresistance measurements. In device fabrication, we first patterned Au/Ge/Ni/Au ohmic contact arrays by electron-beam lithography. Then, the nanotubes are spread from a suspension of Y-junction CNTs ultrasonically dispersed in ethanol. Scanning electron microscopy (SEM) image shows an even distribution of the nanotubes on top of the device region. Single Y-junction CNTs with branches split by 200–300 nm can be found. Then, the GaAs/AlGaAs channel is patterned and etched perpendicularly to the Y-junction CNT. The physical width of channel is $\sim$1 μm. Finally, large Ti/Au contact electrodes are patterned and deposited to connect to the Y-CNT gate and the ohmic contacts. A typical device is shown in Fig. 1, together with a schematic cross-sectional diagram under the Y-CNT gate, which shows the relevant length scales.

After the fabrication, we verified the properties and real electrical width of the channel, by measuring the Shubnikov–de Haas oscillations in the channel with the Y-CNT gate floating in a normal magnetic field B. The minima in the wire resistance plotted against B^{-1} fell on a straight line, yielding $n_{2D}=3.72\times10^{11}$ cm^{-2}, very slightly lower than the original 2DEG density.[6] By assuming the mobility is also largely unchanged, we can estimate the electrical channel width from the channel resistance at $B=0$: We find a depletion width of $\sim$150 nm on both sides of the channel, which is a result of surface states at the exposed GaAs interface.[7]

Our Y-junction multiwalled nanotubes are produced using the chemical vapor deposition method in an anodized aluminum-oxide nanotemplate,[8,9] with a branch diameter of $\sim$40–50 nm. The resistance of the nanotube at low tempera-

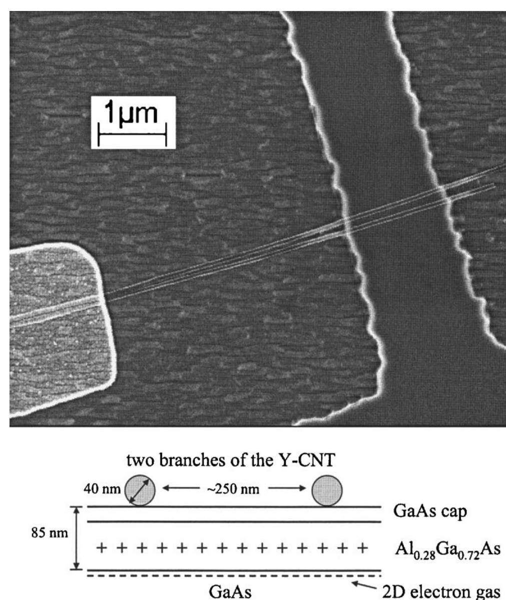

FIG. 1. SEM photograph showing a top view of the Y-junction nanotube dual-gate resonant tunneling FET. The separation of the Y-junction branches that provide the electrostatic double-barrier potential is $\sim$250 nm. A schematic cross-sectional diagram is also shown with the relevant length scales.

[a]Electronic mail: dapeng_wang@brown.edu

0003-6951/2005/87(15)/152102/3/$22.50 © 2005 American Institute of Physics

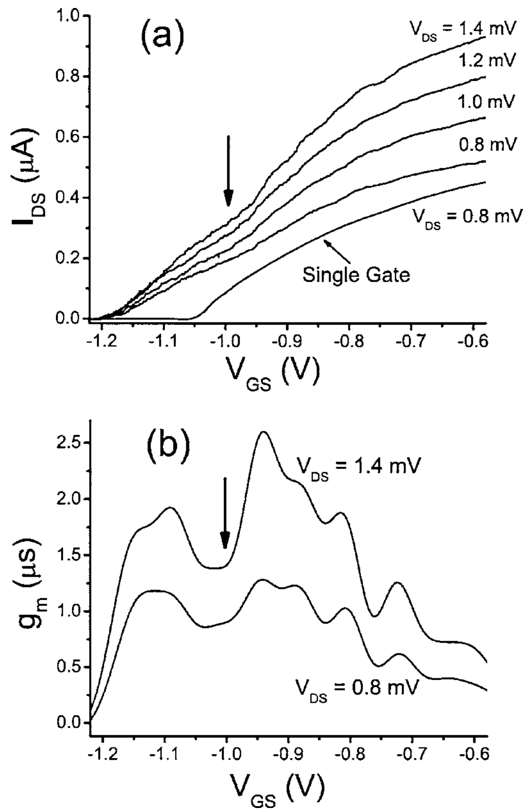

FIG. 2. (a) $I_{DS}(V_{DS}, V_{GS})$ characteristics for fixed V_{DS}=0.8–1.4 mV as a function of V_{GS}, measured at T=4.2 K, showing the step in I_{DS} near V_{GS} =−1 V, as well as weaker fine structures. A single barrier device with a wider gate (where the Y-CNT branches were stuck together) at V_{DS} =0.8 mV is also shown. (b) Transconductance g_m for V_{DS}=0.8 and 1.4 mV at 4.2 K. Arrows mark the I_{DS} step, corresponding to a sharp drop in the transconductance.

ture is negligible compared to the AlGaAs insulating layer between the nanotube and the 2DEG, so we can treat the nanotube as an equipotential at a given V_{GS} bias with respect to the 2DEG. For all measurements reported here, gate leakage is negligible (<10 pA) compared to I_{DS}.

The two branches of the Y-junction nanotube, shown in Fig. 1, biased by $V_{GS}<0$ will create barriers in the 2DEG channel beneath the nanotube. When V_{GS} is negative enough to deplete the 2DEG underneath, the current from source to drain can only flow via tunneling through the confined subbands between the double-barrier potential in the plane of the 2DEG at 4.2 K. The devices can be operated in two different modes. First, we can keep the source-drain voltage V_{DS} fixed and change V_{GS}. The resulting $I_{DS}(V_{DS}, V_{GS})$ transfer characteristics are shown in Fig. 2(a) for several values of V_{DS} in the range from 0.8 to 1.4 mV. The gate voltage V_{GS} is continuously changed, but instead of going smoothly to zero, a steplike structure is evident on each curve around $V_{GS}\sim-1$ V (marked with an arrow) as well as some weaker fine structure. The step can be observed for V_{DS} up to 10 mV. For comparison, the transfer curve of a device with the two Y-CNT branches stuck together, which can be treated as a wider single gate, is also shown in Fig. 2(a) for V_{DS} =0.8 mV. In the single-gate device, I_{DS} falls smoothly to zero at a pinch-off voltage $V_{GS}\sim-1.1$ V, the V_{GS} at which the gate depletes the 2DEG and gate-induced electrostatic barrier is raised above the 2DEG Fermi level E_F.

The transconductance $g_m\equiv\partial I_{DS}/\partial V_{GS}$ of the double-barrier device, calculated by taking the numerical derivative of the transfer characteristic curves, is shown in Fig. 2(b) for V_{DS}=0.8 and 1.4 mV. The main drop in g_m, marked with an arrow in Fig. 2(b), occurs near V_{GS}=−1 V. At this point, the electrostatic double barrier has nearly depleted the 2DEG under the gates and the last one-dimensional (1D) subband confined by the self-consistent parabolic potential passes through the energy window between the E_F in the source and drain (see Fig. 4 and subsequent discussion). Other small features can be clearly seen in the transconductance curves of Fig. 2(b) corresponding to the weaker fine structure in the $I_{DS}(V_{DS}, V_{GS})$ curves of Fig. 2(a). The origin of these fine structure is not yet clear.

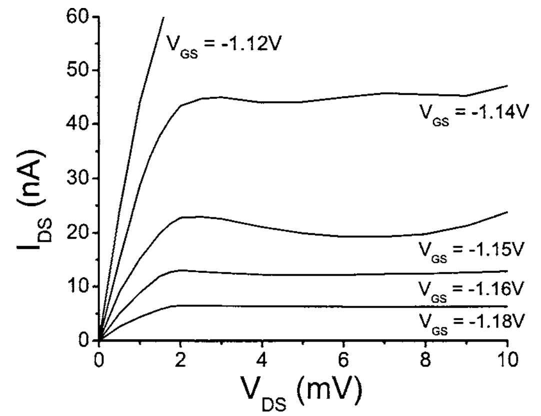

FIG. 3. $I_{DS}(V_{DS}, V_{GS})$ characteristics for fixed V_{GS} as a function of V_{DS} at 4.2 K. A negative differential resistance is seen in a window of V_{GS} values for $V_{DS}>2$ mV. It is strongest for V_{GS}=−1.15 V, but can be seen at more negative V_{GS}, albeit at a reduced current level.

The device can be also measured by varying V_{DS} at a fixed V_{GS} (and hence a fixed electrostatic barrier height). This operation mode resembles that of a standard double-barrier resonant tunneling (RT) diode, where the drain bias is used to tilt the double-barrier potential, and thereby shift the 1D subbands in the well with respect to the occupied 2DEG states in the source. The $I_{DS}(V_{DS}, V_{GS})$ characteristics of the device for several V_{GS} values are shown in Fig. 3. There is a clear region of negative differential resistance for $V_{GS}<-1.14$ V and $V_{DS}>2$ mV, strongest at V_{GS}=−1.15 V but visible at more negative V_{GS}, albeit at reduced current.

As in standard bulk double-barrier RT diodes, electrons tunneling into the restricted density of states conserve energy and transverse momentum (Refs. 10 and 11) (in this device, the only conserved momentum component lies along the CNT barriers—it is perpendicular to both the I_{DS} direction along the channel and the heterostructure growth direction that confines 2DEG vertically). The self-consistent electrostatic problem is quite complex. As a first approximation, we used a two-dimensional (2D) Poisson–Schrödinger modeling program[12] to simulate the electrostatic double-barrier potential and the 1D subband spectrum at V_{DS}=0. Figure 4(a) shows the self-consistently calculated potential profile in the 2DEG plane for the nominal GaAs/AlGaAs heterostructure parameters and V_{GS}=−1.15 V. The calculated 2DEG density $n_{2D}\sim3.3\times10^{11}$ cm^{-2} is somewhat lower than the actual n_{2D}, likely due to uncertainties in the AlGaAs doping and spacer layer thicknesses. The resulting self-consistent double-barrier confining potential is nearly parabolic, with 1D subband energy separation of ~1.5 meV—a value that is essentially determined by the separation of the barriers and not particularly

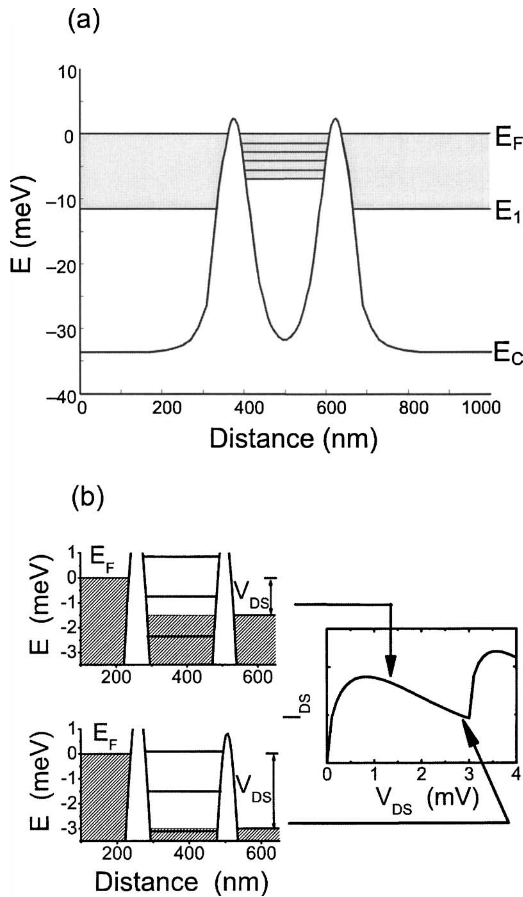

FIG. 4. (a) Self-consistent simulated electrostatic barrier along the 2D electron gas at 4.2 K using a 2D Poisson–Schrödinger modeling program, with $V_{GS}=-1.15$ V. The 1D subbands confined by the electrostatic potential are also shown, which are equally spaced in energy by ~ 1.5 meV. (b) Schematic band diagram for the tunneling I_{DS} at $V_{DS}=1.5$ and 3 meV, together with the simulated current, assuming V_{DS} drops linearly along the double-barrier potential.

sensitive to the exact height of the electrostatic barriers above the 2DEG E_F.

Now consider a small V_{DS} applied to this system, as illustrated in Fig. 4(b). Although the well contains a number of 1D subbands [five for the nominal heterostructure parameters and $V_{GS}=-1.15$ V used in Fig. 4(a)], the subbands that carry the current lie in the eV_{DS} energy window between the E_F in the source and drain. As V_{DS} is increased from zero, the tunneling current I_{DS}, which is a product of the supply function (electrons that can tunnel into the 1D subband conserving energy and transverse momentum) and the transmission coefficient T_S of the source barrier, increases, and then drops. The increase corresponds to more empty states available in the 1D subband as it is lowered with respect to E_F in the source, but there is also a decrease in T_S because the barrier becomes effectively higher. The electrostatic barrier height in our device, similar to the LARTFET devices with lithographic metal gates,[4,5] is broad but quite low [a few meV, see Fig. 4(a)], which is quite different from the 2D-1D-2D tunneling diodes with heterostructure barriers[11] produced by cleaved-edge overgrowth.[13,14] As a result, the decrease in T_S (which, according to the usual Wentzel–Kramers–Brillouin approximation is exponential in the square root of the barrier height) as increasing V_{DS} lowers the 1D subband with respect to the source E_F is significant. The tunneling current I_{DS} [shown in Fig. 4(b)] is calculated, by assuming a symmetric drop of V_{DS} over the double-barrier structure, ignoring the potential drop outside the double-barrier region,[15] and using the barrier potential simulated at $V_{GS}=-1.15$ V [as in Fig. 4(a)]. The qualitative agreement of the first I_{DS} peak with the measured $I_{DS}(V_{DS})$ line shape of Fig. 3 is reasonable. The sharp onset of the second I_{DS} peak would only happen if the second (drain) barrier continued to confine the higher of the two 1D subbands in Fig. 4(b) as V_{DS} is increased, which does not happen for $V_{DS}>5$ mV at the experimental V_{GS}. The current scale of the calculated I_{DS} is arbitrary, as it is highly sensitive to the exact electrostatic barrier height, which we cannot calculate accurately due to uncertainties in the heterostructure parameters.

In conclusion, we have fabricated a variant of a lateral resonant tunneling FET using a multiwalled *Y*-junction CNT to provide the electrostatic double-barrier potential in the plane of a high-mobility 2DEG. We observe structure in the transconductance and negative differential resistance in the $I_{DS}(V_{DS})$ drain circuit characteristic. It would be interesting if CNTs could be used for both the channel and the controlling gate of the device, but the relative positioning of CNTs remains a paramount challenge.

This work was supported by NSF CCF-0403958, NSF ECS-0223943, and ONR. The authors acknowledge the use of the Microelectronics Central Facility at Brown, supported by the NSF MRSEC (DMR-0079964).

[1] A. Javey, J. Guo, Q. Wang, M. Lundstrom, and H. Dai, Nature (London) **424**, 654 (2003).
[2] S. J. Wind, J. Appenzeller, R. Martel, V. Derycke, and P. Avouris, Appl. Phys. Lett. **80**, 3817 (2002).
[3] J. Appenzeller and D. J. Frank, Appl. Phys. Lett. **84**, 1771 (2004).
[4] S. Y. Chou, D. R. Allee, R. F. W. Pease, and J. S. Harris, Jr., Appl. Phys. Lett. **55**, 176 (1989); S. Y. Chou, J. S. Harris, Jr., and R. F. W. Pease, *ibid.* **52**, 1982 (1988).
[5] K. Ismail, D. Antoniadis, and H. I. Smith, Appl. Phys. Lett. **55**, 589 (1989).
[6] K. F. Berggren, G. Roos, and H. van Houten, Phys. Rev. B **37**, 10118 (1988). Our channel is wide enough not to worry about geometric confinement due to its finite width.
[7] K. K. Choi, D. C. Tsui, and K. Alavi, Appl. Phys. Lett. **50**, 110 (1986).
[8] J. Li, C. Papadopoulos, and J. M. Xu, Nature (London) **402**, 253 (2002).
[9] C. Papadopoulos, A. Rakitin, A. S. Vedeneev, and J. M. Xu, Phys. Rev. Lett. **85**, 3476 (2000).
[10] S. Luryi, Appl. Phys. Lett. **47**, 490 (1985).
[11] S. Luryi and F. Capasso, Appl. Phys. Lett. **47**, 1347 (1986).
[12] The simulation code is available from Professor G. L. Snider of University of Notre Dame, see the website ⟨www.nd.edu/~gsnider/⟩ See also G. L. Snider, I.-H. Tan, and E. L. Hu, J. Appl. Phys. **68**, 2849 (1990).
[13] A. Zaslavsky, D. Tsui, M. Santos, and M. Shayegan, Appl. Phys. Lett. **58**, 1440 (1991).
[14] C. Kurdak, D. C. Tsui, S. Parihar, M. B. Santos, H. C. Manoharan, S. A. Lyon, and M. Shayegan, Appl. Phys. Lett. **64**, 610 (1993).
[15] V. J. Goldman, D. C. Tsui, and J. E. Cunningham, Phys. Rev. B **35**, 9387 (1987).